a Tunable, distributed nonlinear resonator

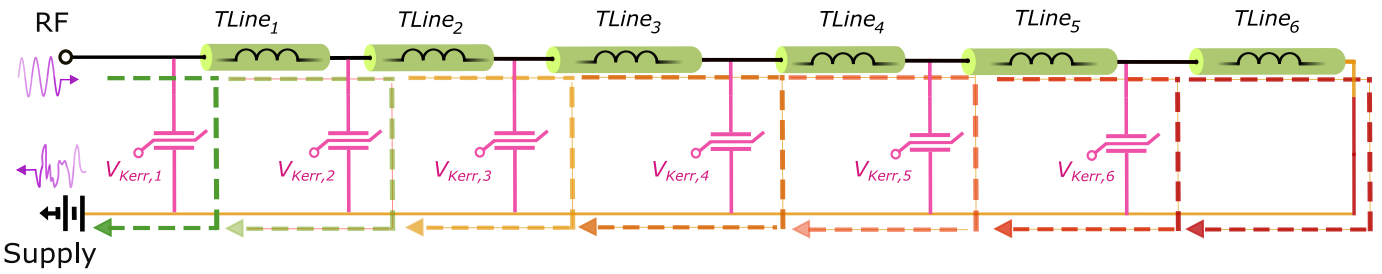

b Top View of Layout

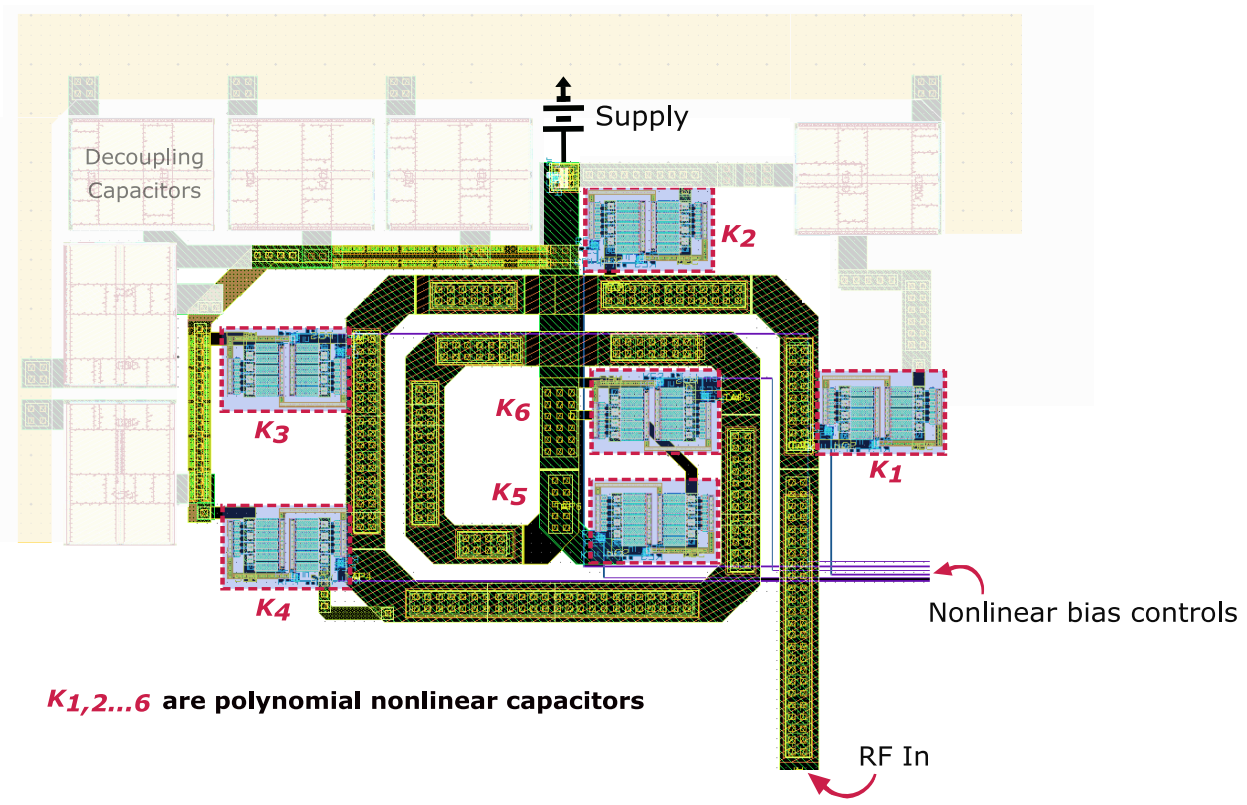

K1,2...6 are polynomial nonlinear capacitors

c Polynomial nonlinear capacitor

c.i

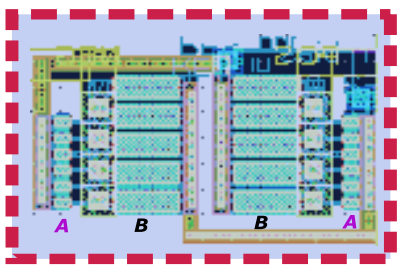

K1,2...6

c.ii

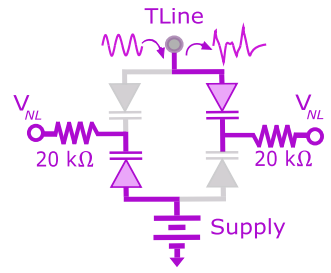

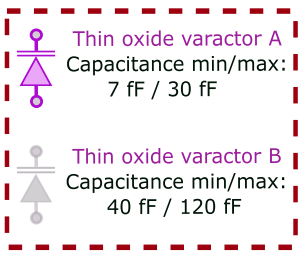

c.iii

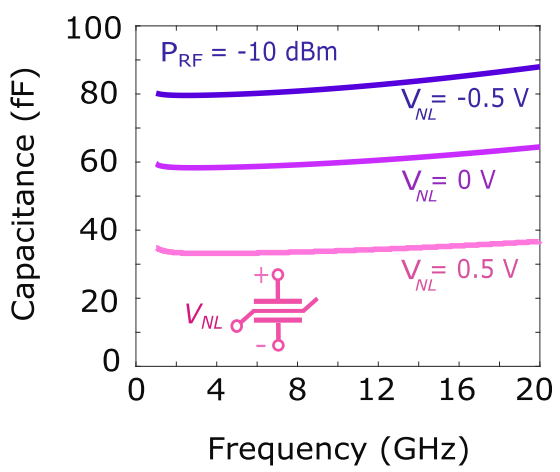

c.iv

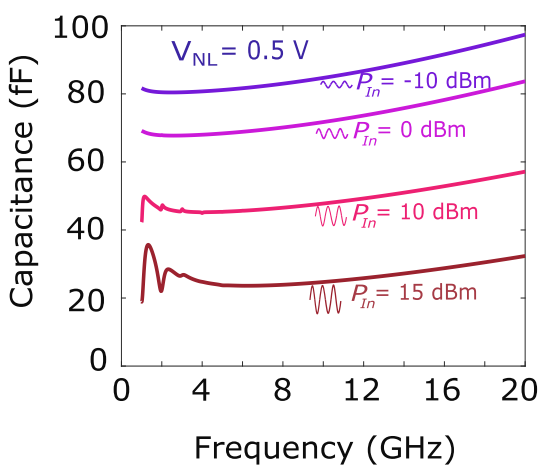

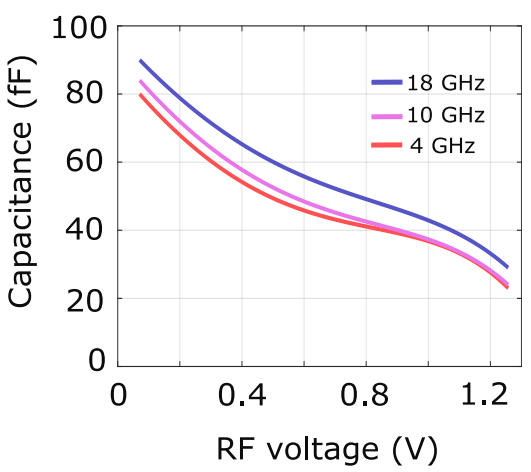

Extended Data Fig 1| Structure of the distributed nonlinear waveguide resonator. a, The nonlinear transmission line comprises cascaded π sections of fixed inductive waveguide segments and drive-sensitive nonlinear capacitors. Each resonance absorbs part of the incoming microwave signal and transmits the rest to subsequent segments. The overall nonlinear response results from cumulative reflections back to RF_{in} port. **b,** Top view of the layout of the nonlinear waveguide. Nonlinear capacitors are inserted periodically along the pretzel-shaped trace. Their nominal bias points are set through analog voltages. **c,** In the Silicon-on-Insulator process used here, a single polynomial nonlinear capacitor consists of two pairs of antiparallel diodes. **c.i,** Compact layout of this component. **c.ii** The schematic, wherein the diode pairs are biased at their mid-point. **c.iii,** SPICE / Spectre-model simulated characterization of the nonlinear capacitor across variation in bias voltages and input RF power shows that by injecting a constant RF input power of -10 dBm, the effective capacitance decreases with increasing bias voltage. **c.iv,** The effective capacitance is highly sensitive to the input RF drive's power. The capacitance reduces with increasing field strength. **c.v,** The same nonlinearity, when considering its variance for different frequencies. Here, the capacitance varies with RF voltage as $C_{eff}(V_{NL}, V_{in}) = a - b\,V_{in} + c\,V_{in}^2 - d\,V_{in}^3 + \ldots$ fF which is well-suited to generating expansive functions for a neural pre-processor.

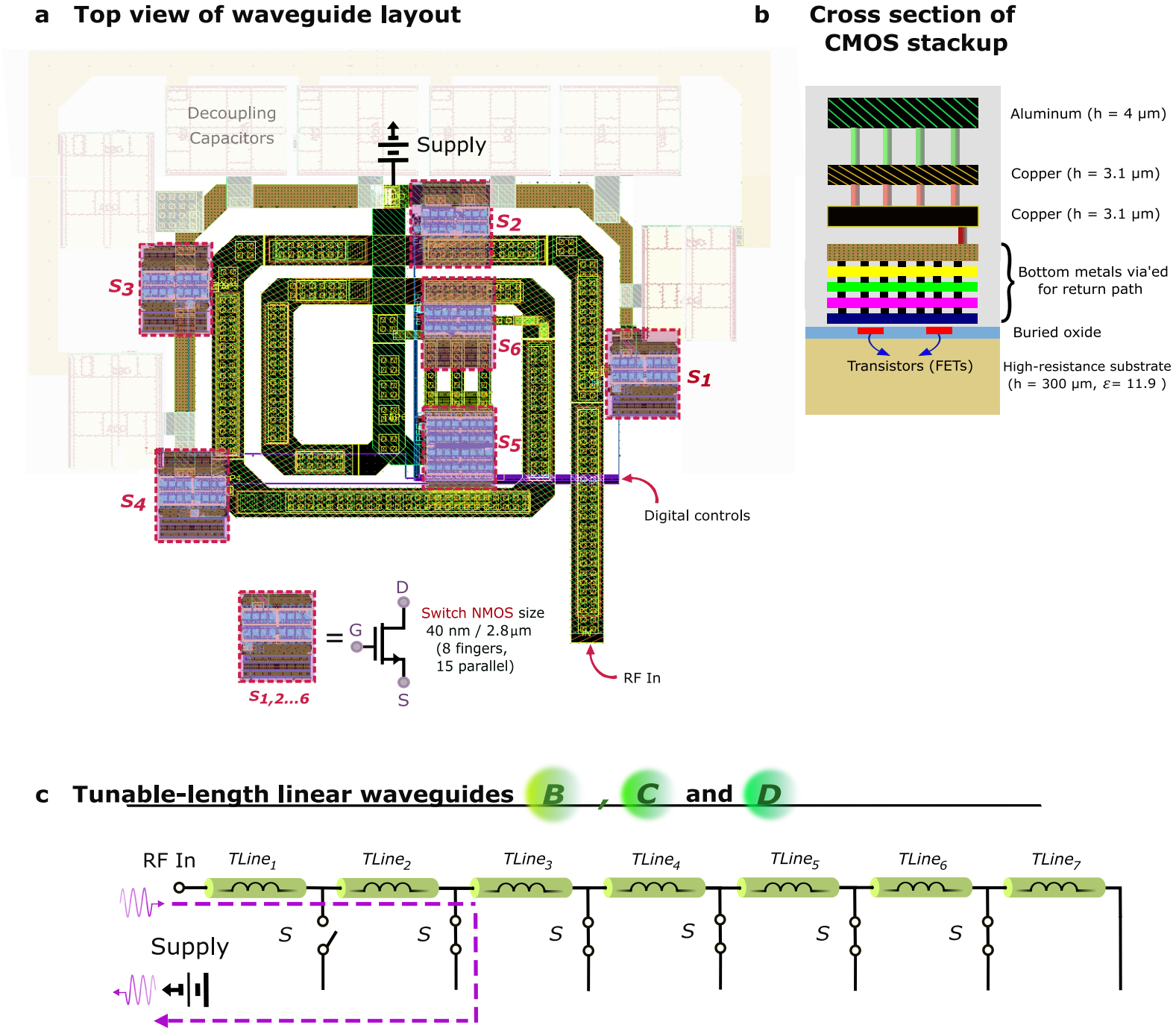

Extended Data Fig 2| Structure of the distributed linear waveguide a, Top view of the layout of the tunable waveguide that produces linear modes *B, C* and D. Switches $S_{1,2....6}$ are inserted periodically along the length the transmission line and makes it tunable in length, with subsegments $TLine_{1,2...6}$. Shorting the line through these switches alters the effective length of the waveguide to support different fundamental frequencies. **b,** Cross-section of RF-optimized and digital metal layers in the 45 nm Silicon-on-Insulator CMOS metal stack. Here, the top three layers are via'ed together for low-loss transmission. The five metal layers below are used for routing control signals from a Serial-to-Parallel Interface, to the switches, and also via'ed together to form a low-loss return path to the power supply. **c,** A schematic of the linear waveguide resonators, with options to lengthen or shorten the return path of the microwave signal. In the experiments, however, for simplicity, only the shortest path (configuration with all switches turned on) was used for training in the machine learning tasks.

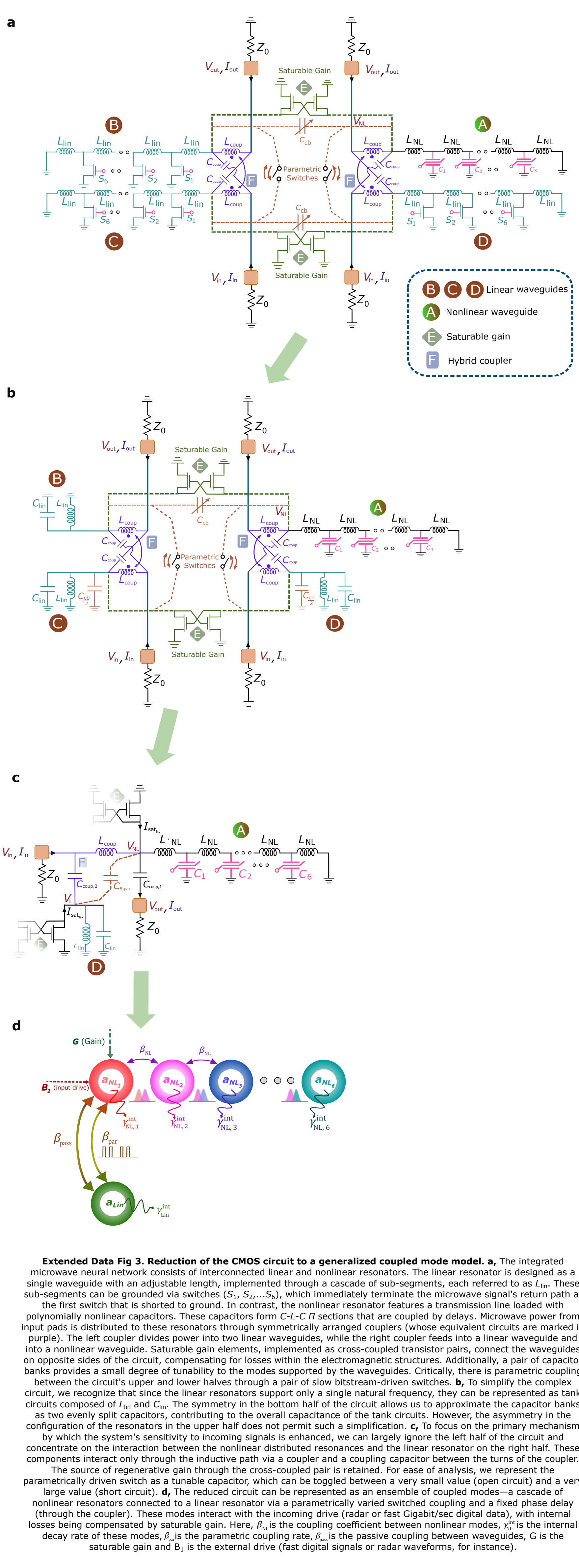

Extended Data Fig 3. Reduction of the CMOS circuit to a generalized coupled mode model. a, The integrated microwave neural network consists of interconnected linear and nonlinear resonators. The linear resonator is designed as a single waveguide with an adjustable length, implemented through a cascade of sub-segments, each referred to as L_{lin}. These sub-segments can be grounded via switches (S_1, S_2,...S_6), which immediately terminate the microwave signal's return path at the first switch that is shorted to ground. In contrast, the nonlinear resonator features a transmission line loaded with polynomially nonlinear capacitors. These capacitors form *C-L-C Π* sections that are coupled by delays. Microwave power from input pads is distributed to these resonators through symmetrically arranged couplers (whose equivalent circuits are marked in purple). The left coupler divides power into two linear waveguides, while the right coupler feeds into a linear waveguide and into a nonlinear waveguide. Saturable gain elements, implemented as cross-coupled transistor pairs, connect the waveguides on opposite sides of the circuit, compensating for losses within the electromagnetic structures. Additionally, a pair of capacitor banks provides a small degree of tunability to the modes supported by the waveguides. Critically, there is parametric coupling between the circuit's upper and lower halves through a pair of slow bitstream-driven switches. **b,** To simplify the complex circuit, we recognize that since the linear resonators support only a single natural frequency, they can be represented as tank circuits composed of L_{lin} and C_{lin}. The symmetry in the bottom half of the circuit allows us to approximate the capacitor banks as two evenly split capacitors, contributing to the overall capacitance of the tank circuits. However, the asymmetry in the configuration of the resonators in the upper half does not permit such a simplification. **c,** To focus on the primary mechanism by which the system's sensitivity to incoming signals is enhanced, we can largely ignore the left half of the circuit and concentrate on the interaction between the nonlinear distributed resonances and the linear resonator on the right half. These components interact only through the inductive path via a coupler and a coupling capacitor between the turns of the coupler. The source of regenerative gain through the cross-coupled pair is retained. For ease of analysis, we represent the parametrically driven switch as a tunable capacitor, which can be toggled between a very small value (open circuit) and a very large value (short circuit). **d,** The reduced circuit can be represented as an ensemble of coupled modes—a cascade of nonlinear resonators connected to a linear resonator via a parametrically varied switched coupling and a fixed phase delay (through the coupler). These modes interact with the incoming drive (radar or fast Gigabit/sec digital data), with internal losses being compensated by saturable gain. Here, β_{NL} is the coupling coefficient between nonlinear modes, γ_{NL}^{int} is the internal decay rate of these modes, β_{par} is the parametric coupling rate, β_{pass} is the passive coupling between waveguides, G is the saturable gain and B_1 is the external drive (fast digital signals or radar waveforms, for instance).

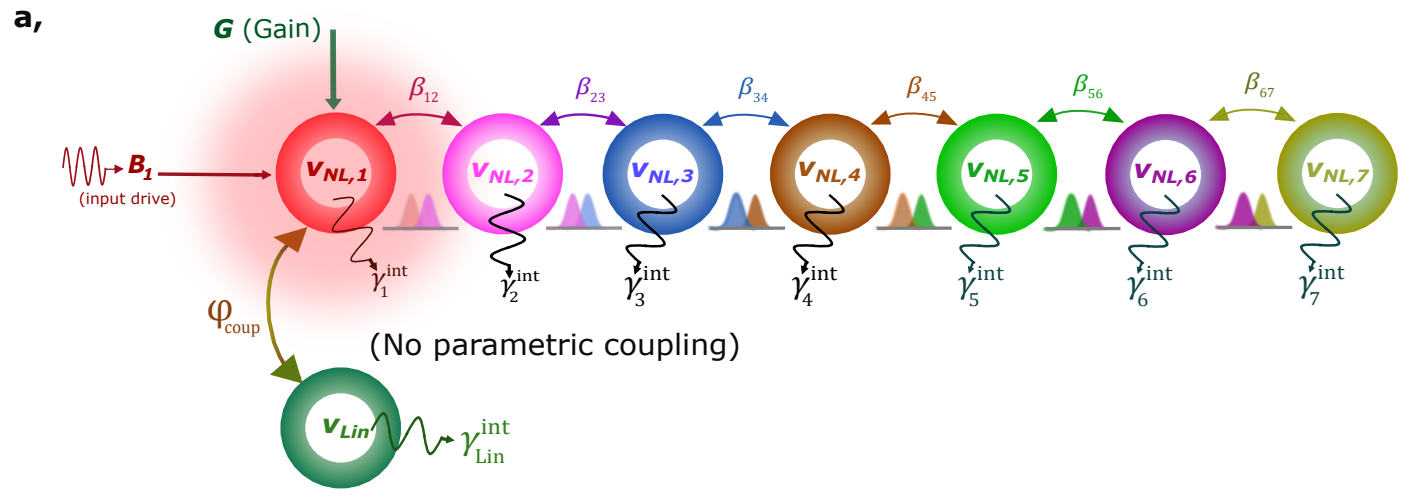

b.i Initial conditions with drive at $0.5\times\omega^{o}_{NL,1}$

$v^{o}_{NL,1}$=0.8+0.6j *V* $v^{o}_{NL,5}$ =0.3+0.6j *V*
$v^{o}_{NL,2}$= 0.5+0.5j *V* $v^{o}_{NL,6}$ = 0.5+0.5j *V*
$v^{o}_{NL,3}$= 0.2+0.4j *V* $v^{o}_{NL,7}$ = 0.2+0.4j *V*
$v^{o}_{NL,4}$= 0.8+0.6j *V* v^{o}_{Lin} = 0.3+0.6j *V*

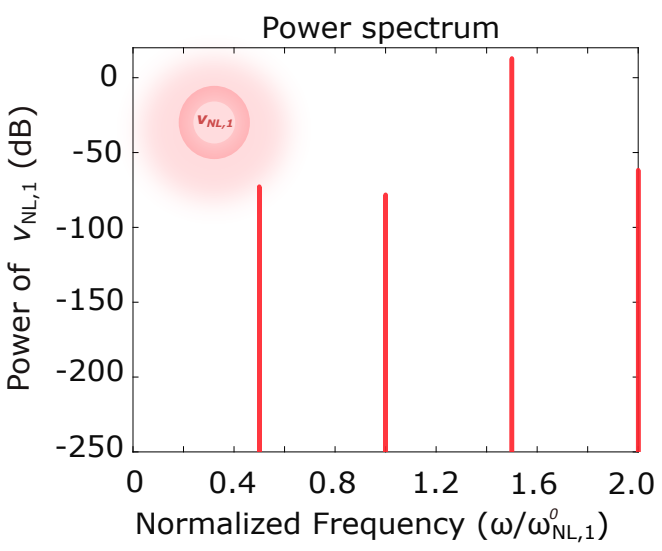

b.ii Different initial conditions with drive at $0.5\times\omega^{o}_{NL,1}$

$v^{o}_{NL,1}$=0.8+0.8j *V* $v^{o}_{NL,5}$ =0.6+0.1j *V*
$v^{o}_{NL,2}$= 0.3+0.1j *V* $v^{o}_{NL,6}$ = 0.6+0.9j *V*
$v^{o}_{NL,3}$= 0.4+0.3j *V* $v^{o}_{NL,7}$ = 0.3+0.6j *V*
$v^{o}_{NL,4}$= 0.3+0.9j *V* v^{o}_{Lin} = 0.6+0.7j *V*

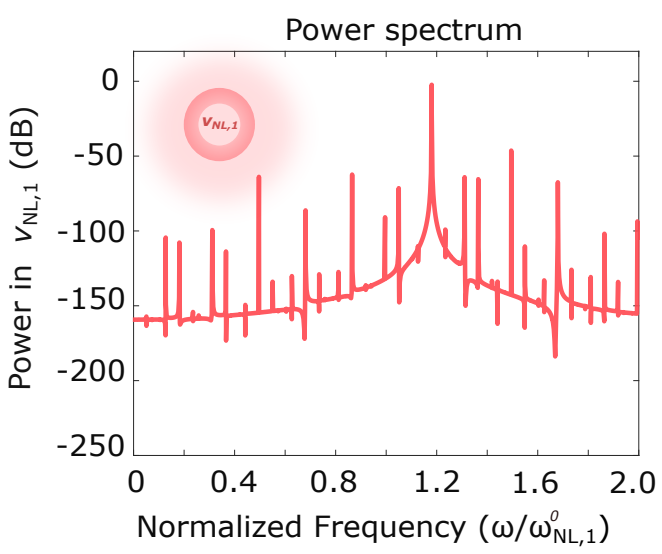

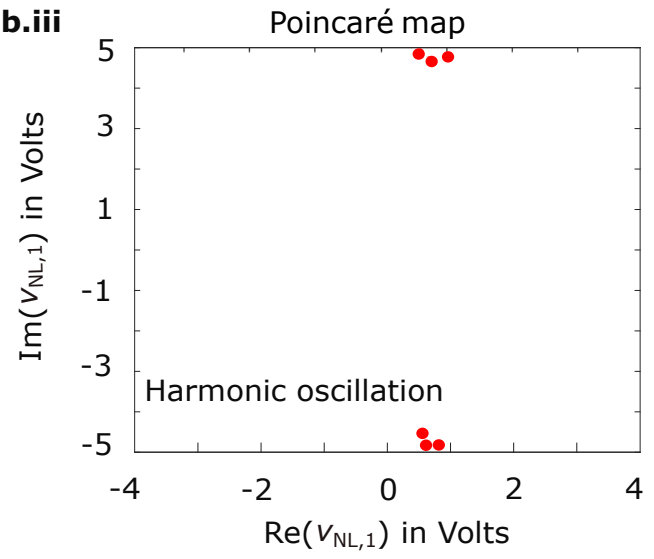

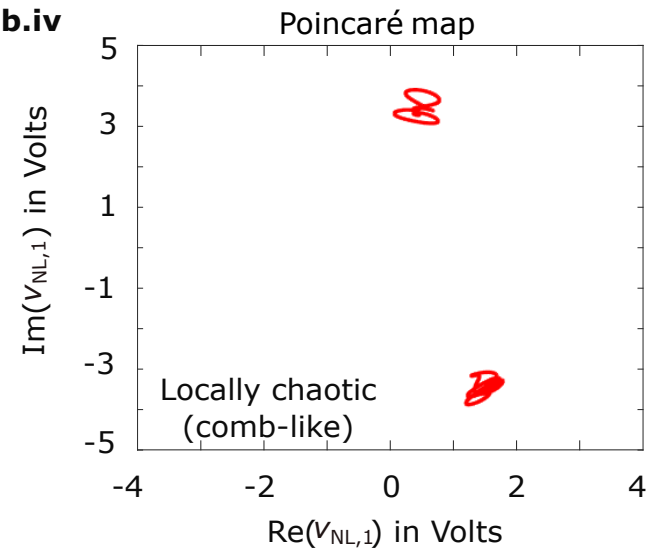

c.i Initial conditions with drive at $0.65\times\omega^{o}_{NL,1}$

$v^{o}_{NL,1}$=0.5+0.8j *V* $v^{o}_{NL,5}$ =0.1+0.8j *V*
$v^{o}_{NL,2}$= 0.9+0.3j *V* $v^{o}_{NL,6}$ = 0.6+0.3j *V*
$v^{o}_{NL,3}$= 0.7+0.8j *V* $v^{o}_{NL,7}$ = 0.5+0.8j *V*
$v^{o}_{NL,4}$= 0.5+0.7j *V* v^{o}_{Lin} = 0.4+0.6j *V*

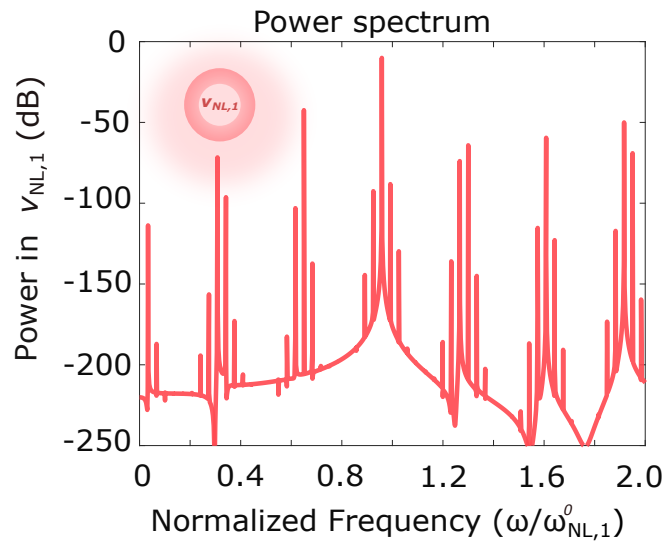

c.ii Different initial conditions with drive at $0.65\times\omega^{o}_{NL,1}$

$v^{o}_{NL,1}$=0.9+0.1j *V* $v^{o}_{NL,5}$ =0.8+0.5j *V*
$v^{o}_{NL,2}$= 0.8+0.9j *V* $v^{o}_{NL,6}$ = 0.7+0.9j *V*
$v^{o}_{NL,3}$= 0.7+0.9j *V* $v^{o}_{NL,7}$ = 0.2+0.7j *V*
$v^{o}_{NL,4}$= 0.4+0.2j *V* v^{o}_{Lin} = 0.1+0.9j *V*

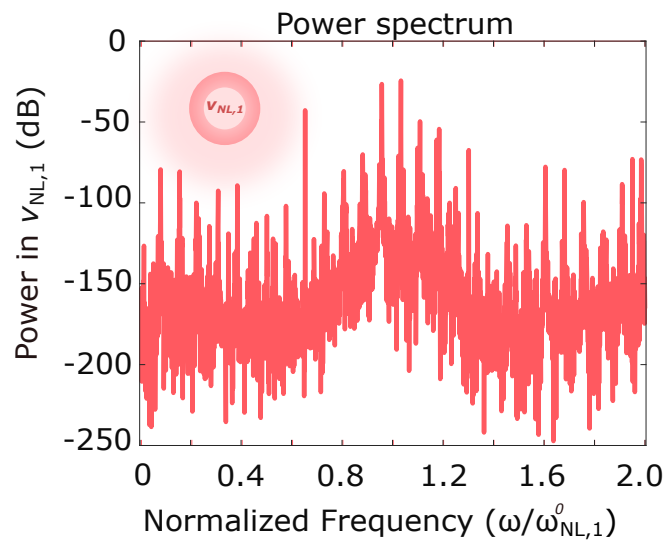

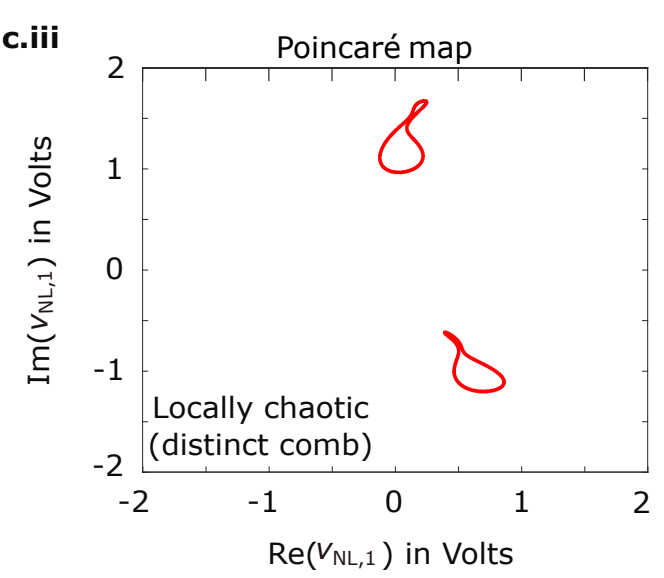

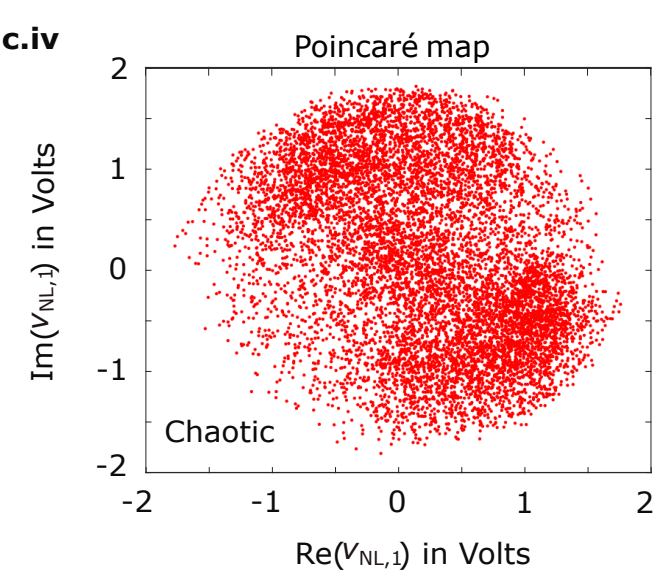

Extended Fig. 4 | Effects of initial conditions and drive-detuning on spectral response and evolution of memory-like dynamics in the Microwave Neural Network, without parametric switch coupling. Power spectrum and the Poincaré map of modes within the first nonlinear resonator ($\boldsymbol{v_{NL,1}}$) are observed. **(b)** The MNN is driven with an external signal at $0.5\omega_{NL,1}$. For a first set of initial conditions imposed on individual resonators' responses, there exists a regime in which pure harmonic oscillation is seen (**b.i**) and for another set of initial conditions, comb-like behavior is produced (**b.ii**). These correspond to situations where the Poincaré map shows sparse and organized points. This suggests a quasi-stable dynamic state **(b.iii)** and another where the two islands reflect more unstable, dynamic responses **(b.iv)**, indicating locally chaotic solutions. **(c)** If, instead, the drive was fed to the MNN at $0.65\omega_{NL,1}$, different working regimes are triggered by different initial conditions. True comb-like behavior **(c.i)** can be produced, as evidenced by isolated, longer-memory, coherent solutions on the Poincaré map **(c.iii)**. In another instance, divergent chaotic behavior shown by dense, scattered points (indicative of chaotic dynamics) **(c.iv)** manifests itself by a less structured spectrum emitted by the nonlinear resonator(s) **(c.ii)**. For all simulations, nonlinear coupling coefficients, gain and decay rates are normalized with respect to $\omega_{\mathbf{NL,1}}$. Here, $\beta_{i,i+1}$ =0.02 and γ_i^{int} =0.03, with ***i***=1,2...7 and saturable gain, ***G***, equals 0.2. Since parametric coupling is absent, β_{par} = 0.

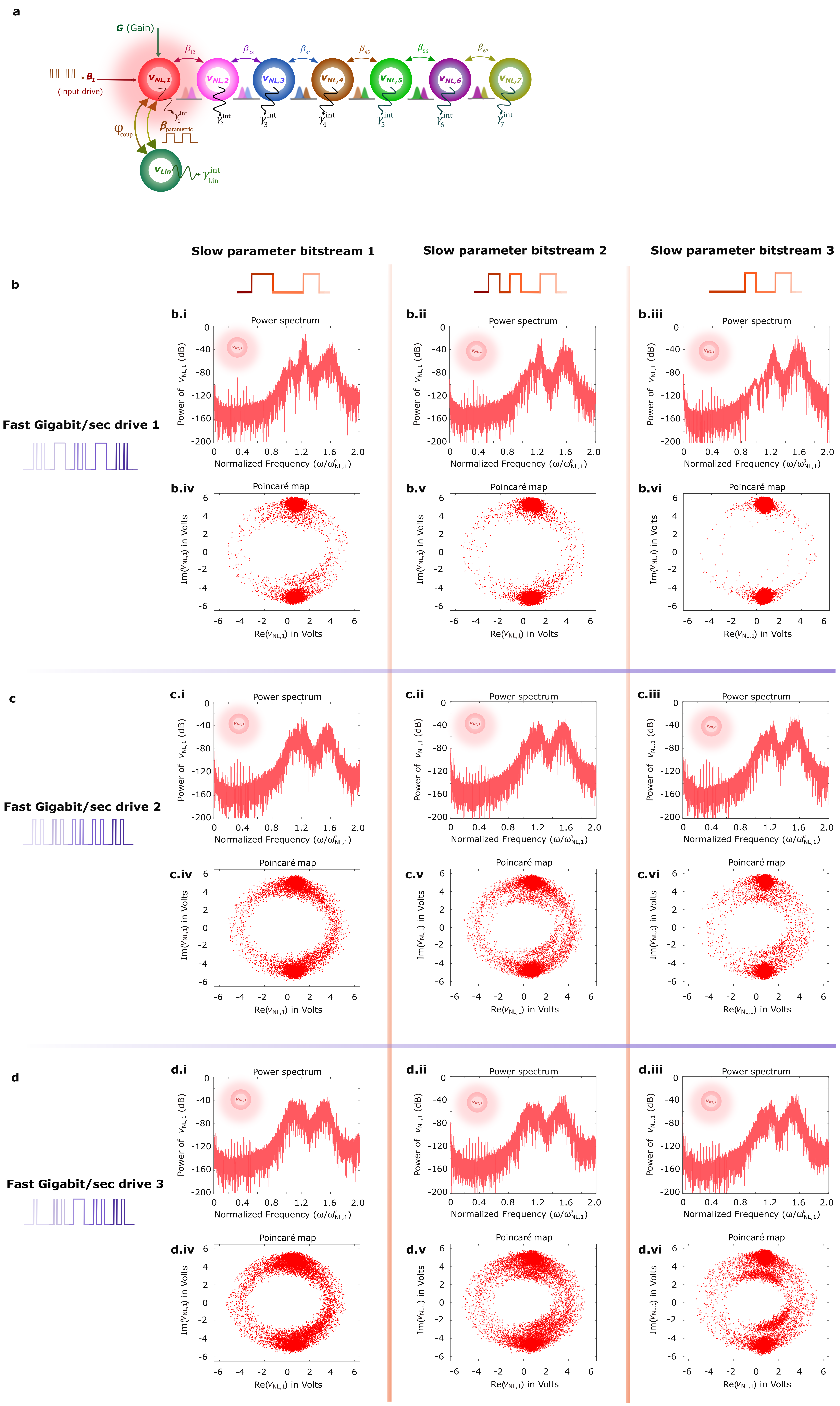

Extended Data Fig. 5 | Manipulation of the comb-like spectra emitted by the Microwave Neural Network, with microwave-speed signals and slow parametric bitstreams. **a,** In the experiments involving Gigabit/sec data and radar returns, the accessible phase space of the MNN, in terms of the real and imaginary components of the resonators' modes, is constrained by the configurations of incoming drive signals and the parametric modulation applied on the switch between the first non-linear mode and a linear mode. **b** and **c,** The output spectra and Poincaré maps. For Drive 1, the Poincaré map for slow parameter bitstreams 1 and 2 shows clustered points with a few points that are more spread out (**b.iv** and **b.v**), suggesting quasi-periodic dynamics while Bitstream 3 gives tightly clustered points (**b.vi**), indicating stable, periodic behavior. For Drive 2, under action of all three parametric bitstreams, the formation of ring-like structures indicates quasi-periodic behavior with non-linear dynamics (**c.iv**, **c.v** and **c.vi**). Finally, under Drive 3, the Poincaré maps, parametric bitstreams 1 and 2 produce a combination of ring-like patterns and clustered points (**d.iv** and **d.v**), revealing a tendency towards chaotic behavior, while Bitstream 3 exhibits multiple, structured rings, indicating quasi-periodic behavior with complex and unstable dynamics (**d.vi**). For all simulations, nonlinear coupling coefficients, gain and decay rates are normalized with respect to $\omega_{NL,1}$. Here, $\beta_{i,i+1}$ =0.02. γ^{i}_{int} =0.03, with i=1,2...7 and saturable gain, G, equals 0.2.

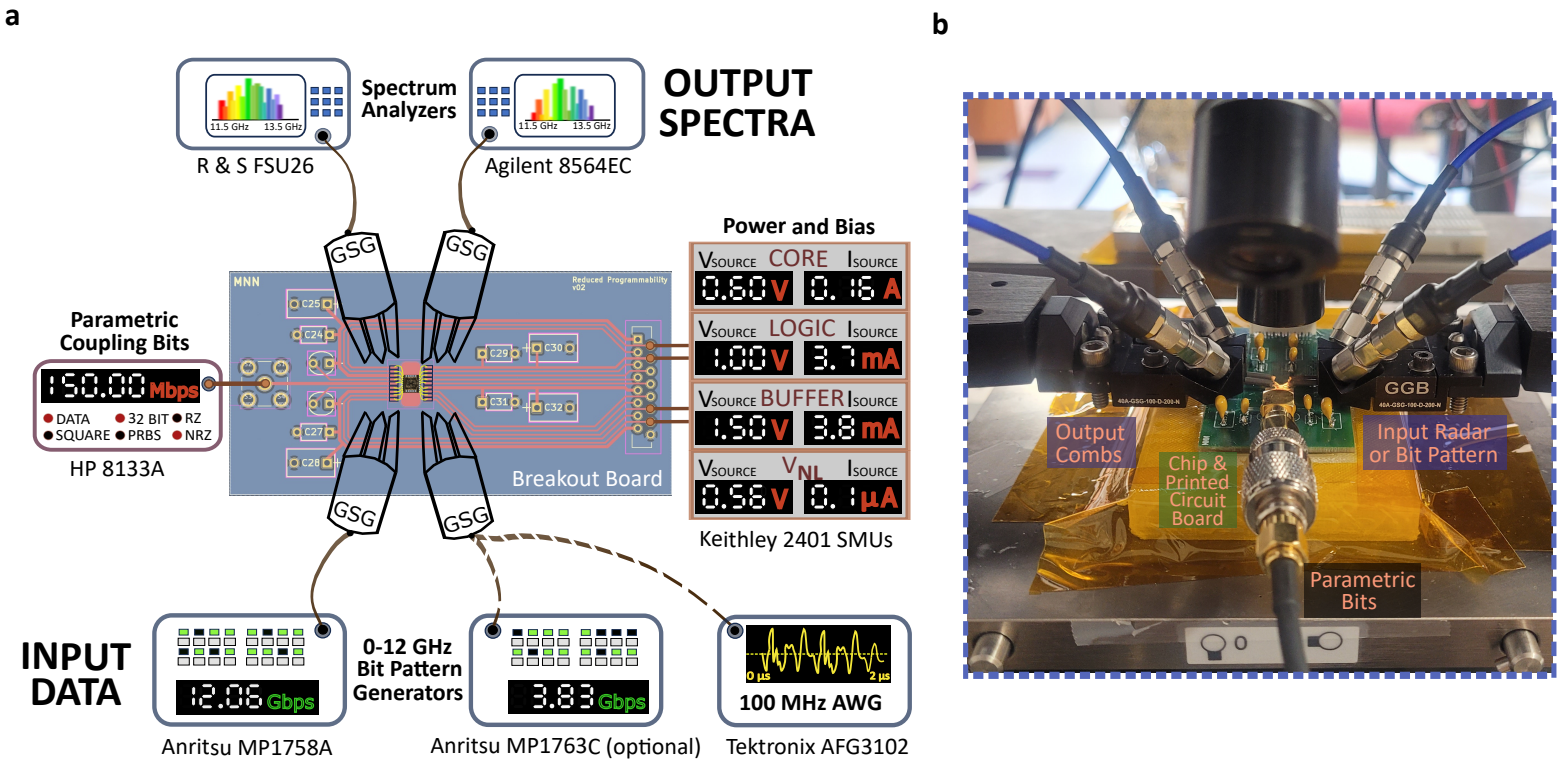

Extended Data Figure 6. Experimental setup to record the MNN's response to microwave drives and parametric bitstreams. The CMOS MNN chip is wire-bonded to a Printed Circuit Board, which connects it to external power supplies and bias voltages for the oscillators' core, logic and drivers and nonlinear capacitors' bias. **a,** A low-speed parametric bit pattern (at 150 MBit/sec) drives switches that establish parametric coupling between linear and nonlinear oscillators. A first pair of probes, forming a Ground-Signal-Ground-Signal-Ground (GSGSG) configuration cyclically transfers high bandwidth 0-12 GBit/sec bitstreams into the chip to interact with the default comb-like response. The resulting microwave computations are manifested as new comb-like spectra. These output spectra, from two ports, are read off spectrum analyzers in smaller bands of about two or three gigahertz, through a second pair of probes and Ground-Signal-Ground-Signal-Ground waveguides. **b,** The probe-station assembly consists of the CMOS die attached to a breakout PCB, interfaced with millimeter wave probes for input and output data and power supplies. It also includes a low-speed BNC cable interface for feeding in the parametric bitstream.

a. Spectra formed by variations in saturable gain supply voltage, with a constant nonlinear bias (V_{NL}) = 0.2 V

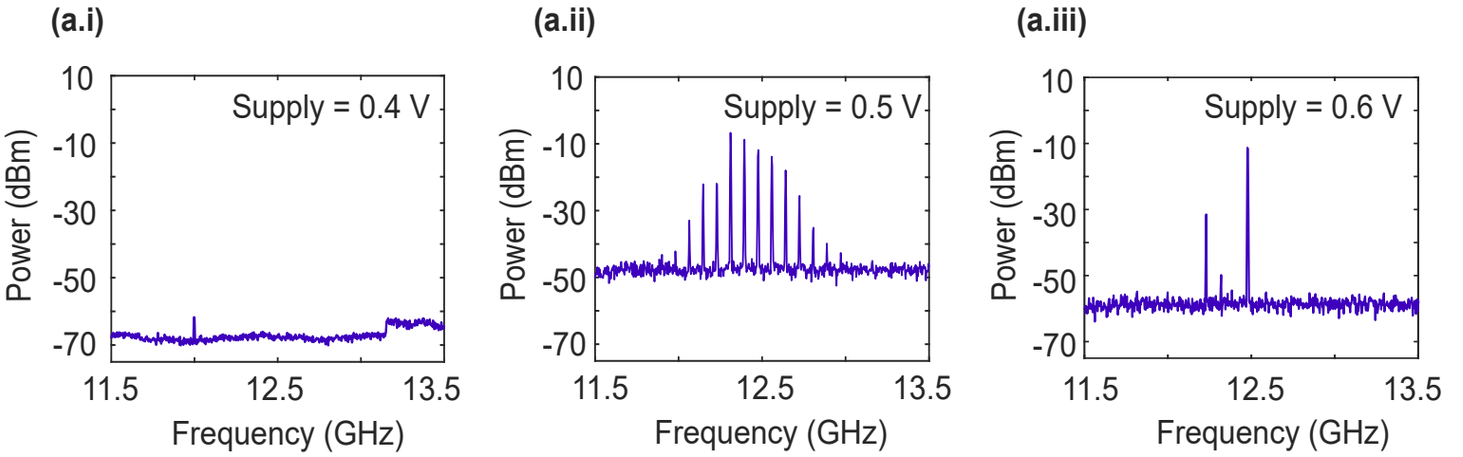

b. Spectra formed by variations in nonlinear bias (V_{NL}) with a constant supply voltage = 0.5 V

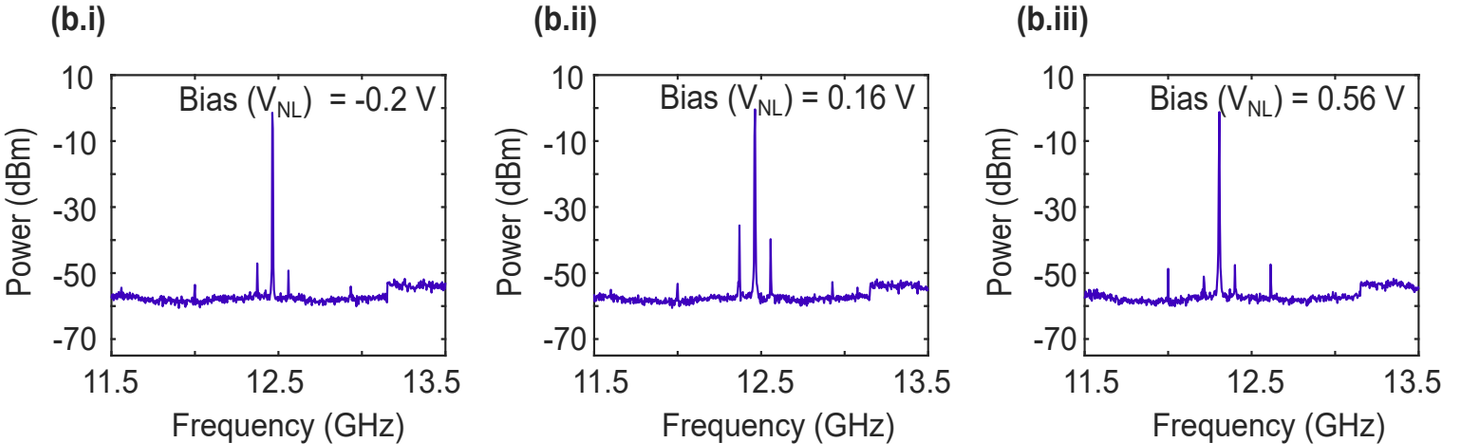

c. Comb-like spectra reshaped by variations in slow (50 MHz) parametric bits, at V_{NL} = 0.56 V and supply = 0.5 V

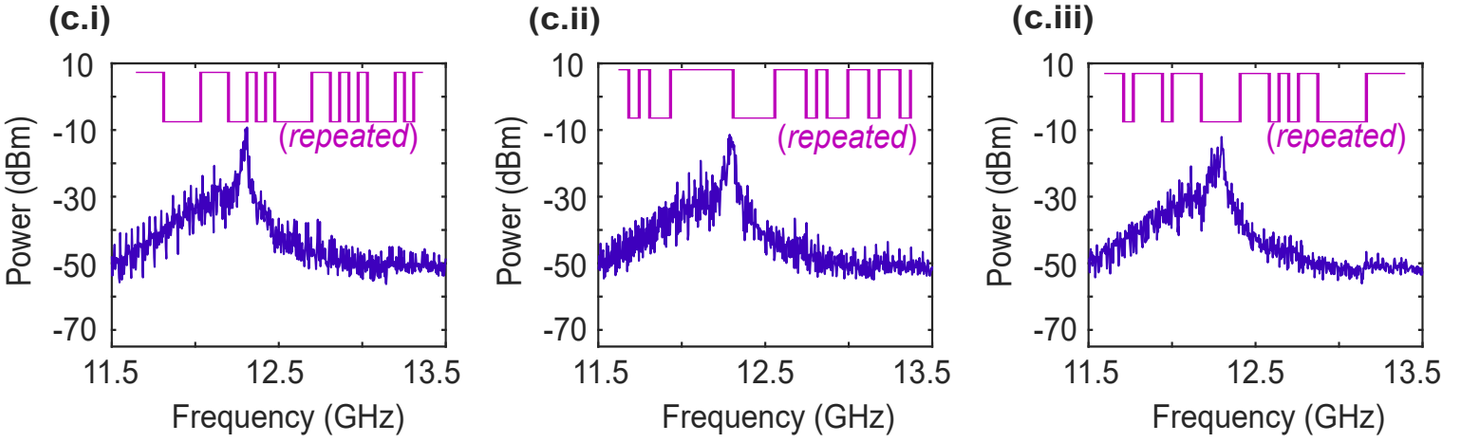

Extended Data Figure 7. Measured frequency-comb-like spectra generated by the coupled nonlinear and linear resonators. **a,** The supply voltage on the saturable gain element alters the transconductance of the cross-coupled pair's transistors and, thereby, the stability of the comb. It has a nominal value of 0.5 V, below which it collapses. **b,** The polynomial nonlinearity is tuned using bias voltages that set the sensitivity of the transmission line's capacitances to incoming microwaves. **c,** The inherent response can be altered by feeding parameters through a 32-bit sequence, run cyclically at slow speeds under 150 MHz. In the experiment, this parameterized comb is exposed to incoming drive signals and performs computation on them.

a Measured power spectrum of undisturbed comb

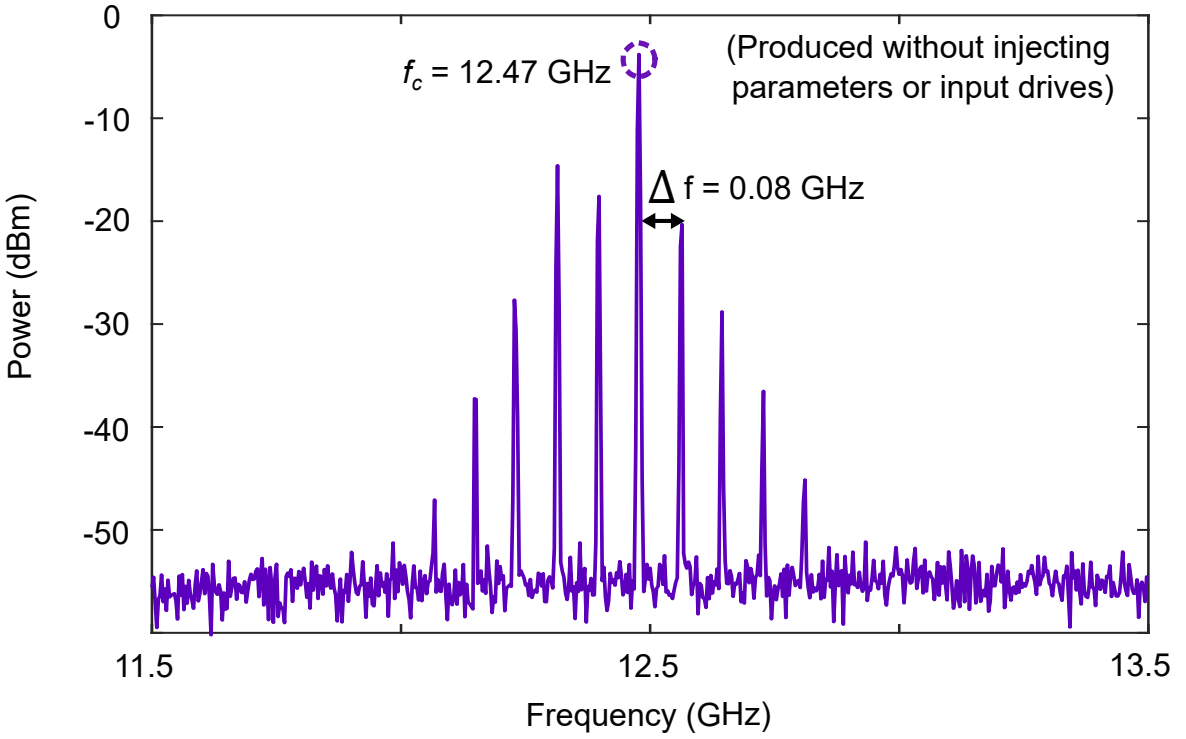

b Measured Phase Noise

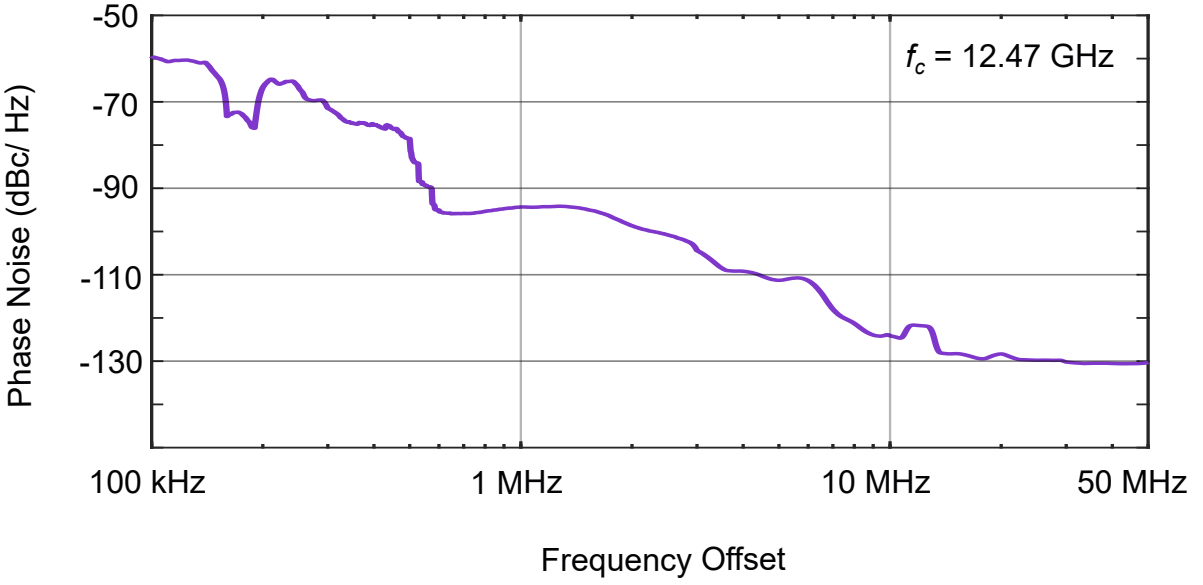

Extended Data Figure 8. Characterization of the comb generated by coupling of nonlinear modes on chip. a, Under nominal biasing conditions (power supply of 0.6 V and V_{NL} = 0.6 V) and without the influence of parametric bits and incoming microwave signals, the measured frequency comb is centered at 12.47 GHz and has a constant line spacing of 80 MHz. **b,** The phase noise is measured for various offsets from the central component. While it has slightly higher close-in noise than conventional CMOS oscillators, microwave neurons built from this modality are stable and highly sensitive to drive signals.